Electronic Supplementary Material (ESI) for Journal of Materials Chemistry A.

Constructing interface synergistic effect from MoS_2/SnS heterojunction decorating N, S co-doped carbon nanosheets with enhanced sodium ion storage performance

Lisan Cui[a], Chunlei Tan[a], Guanhua Yang[b], Yu Li[a], Qichang Pan[a,c,*], Man Zhang[a], Zilu Chen[a], Fenghua Zheng[a,c,*], Hongqiang Wang[a,c], Qingyu Li[a,c]

a Guangxi Key Laboratory of Low Carbon Energy Materials, School of Chemical and Pharmaceutical Science, Guangxi Normal University, Guilin, 541004, China.

b School of Mechanical and Transportation Engineering, Guangxi University of Science and Technology, Liuzhou 545006, China.

c Guangxi New Energy Ship Battery Engineering Technology Research Center, Guangxi Normal University, Guilin, 541004, China.

Corresponding author.

E-mail addresses: panqc0526@163.com (Q. Pan), zhengfh870627@163.com (F. Zheng).

Experimental section

Synthesis

In a typical synthesis, 1.04 g $Na_2SnO_3 \cdot 3H_2O$, 0.45 g $Na_2MoO_4 \cdot 2H_2O$, 2.25 g $CS(NH_2)_2$, 4 g $(NH_4)_3C_6H_5O_7$ and 10 g NaCl were added to in 40 ml deionized water to form a uniform mixed solution under magnetic stirring. Subsequently, the solution were dried by freeze-dried. Then, the precursor was calcined at 750 ^oC for 4 h under Ar atmosphere and washed with deionized water to obtain SnS/MoS_2/NS-CNs. For comparison, the SnS/NS-CNs and MoS_2/NS-CNs were prepared under the same conditions without added molybdenum sources and tin sources. And the carbon nanosheets were synthesized only added carbon sources.

Characterization

Structural and morphological analyses of the synthesized composites were performed using SEM (TESCAN, VEGA3 and SU8220) and TEM (JEOL, JEM-F2100). The crystal structures and phases were analyzed using XRD (Rigaku D/ max-Ⅲ, Cu-Kα). The specific surface areas and pore-size distributions of the samples were estimated via BET (Quantachrome Instumenta Autosorb-iQ2-MP) analysis of nitrogen-adsorption measurements. The chemical states of the SnS/MoS_2/NS-CNs and SnS/NS-CNs composite were confirmed using XPS (Thermo Scientific K-Alpha, Al-Kα, 12 kV and 20 mA). The SnS and MoS_2 content of the SnS/MoS_2/NS-CNs and SnS/NS-CNs composite was determined via TG (SDT Q600) and ICP-OES/MS (Agilent 7700s). Raman spectroscopy (Renishaw system 1000) was conducted at

room temperature to study the nature of the carbon, SnS and MoS_2 nanosheets of the SnS/MoS_2/NS-CNs composite.

Electrochemical Measurements

The sodium ion storage performance was tested via assembled 2032-type coin cells. The sample powders (active material, 70 wt%), Super P (conducting agent, 15 wt%), sodium carboxymethyl cellulose (binder, 15 wt%) and distilled water via mechanical mixing to prepare anode material slurry. To prepare the working electrode, the slurry was evenly coated the surface of the copper foil, Then dried at 80 ^{o}C for 24 h. The diameter of the round electrode was 12 mm, and the mass loading of electrode is about 1.0 mg cm^{-2}. Sodium foil, Glass fibre were employed as the counter electrode and separator, respectively. The electrolyte contain 1 M of $NaPF_6$ dissolved in ethylene carbonate (EC)/Diethyl Carbonate (DEC) (1:1 volume) with fluoroethylene carbonate (FEC) (5 wt%). Galvanostatic charge/discharge measurements (0.01-3.0 V vs. Na^+/Na) were conducted at battery test system (LAND CT2001A). Cyclic voltammetry (CV) and electrochemical impedance spectroscopy (EIS) was performed on a electrochemical workstation (Zahner, IM6) in the frequency range of 0.01 Hz-100 kHz. The cells after the cycling performance were disassembled in glove box with argon-filled, and the working electrodes cleaned by DMC and dried in vacuum oven for the following characterizations.

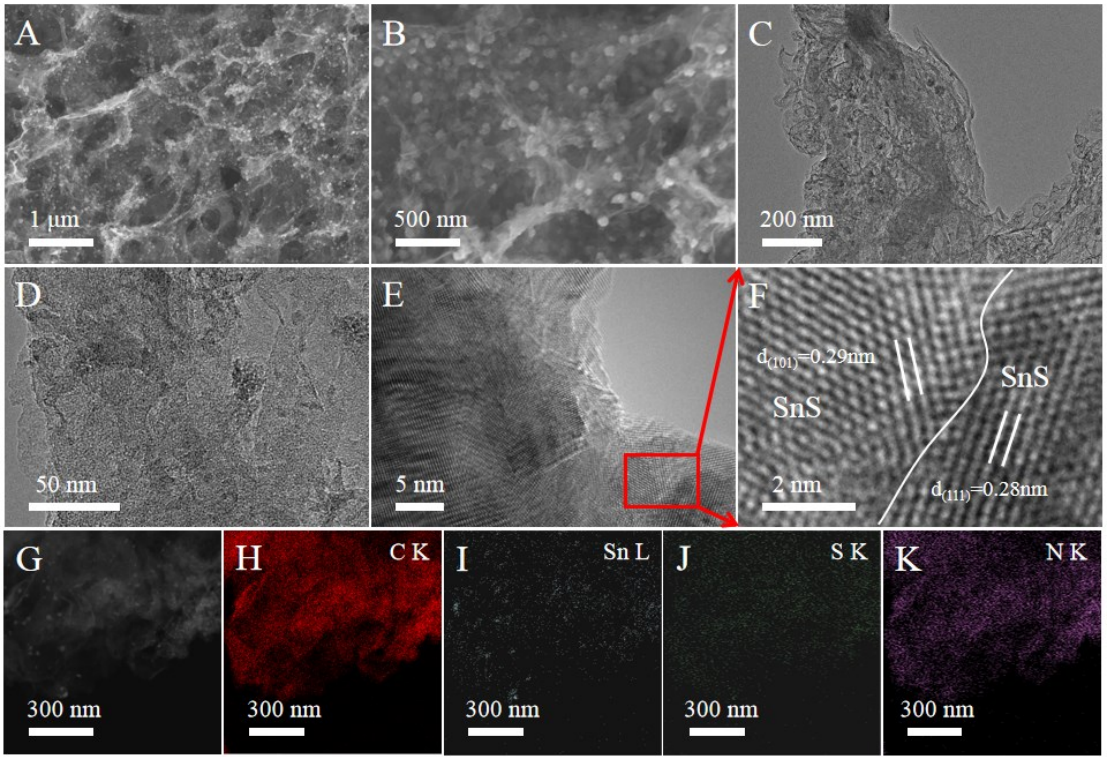

Fig. S1 SEM images of SnS/NS-CNs with different magnifications (A and B). TEM images of SnS/NS-CNs with different magnifications (C-F) and elemental mapping images of SnS/NS-CNs (G-K).

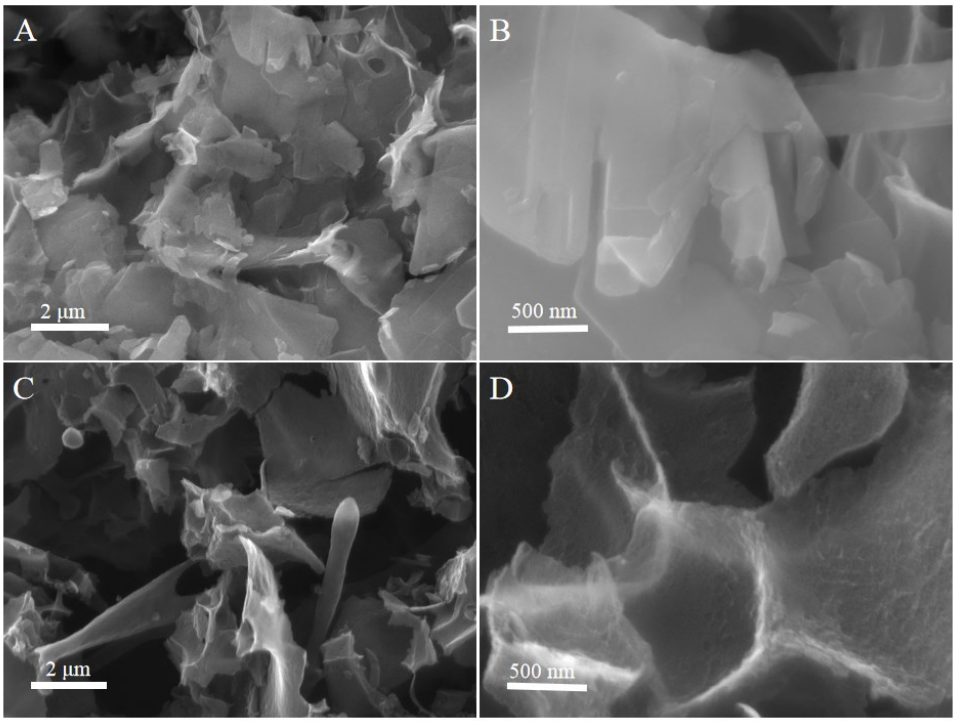

Fig. S2 SEM images of MoS_2/NS-CNs (A and B) and NS-CNs with different magnifications (C and D).

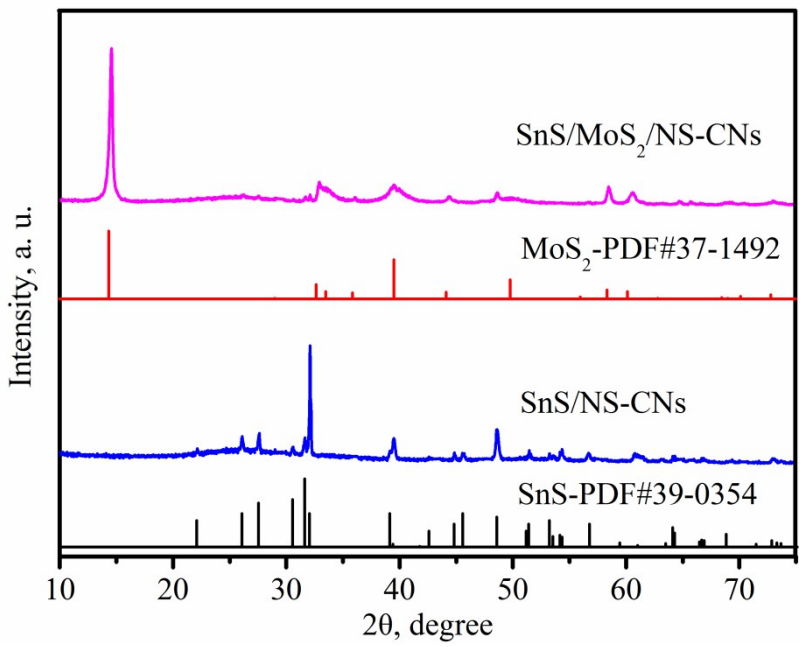

Fig. S3 XRD patterns of SnS/MoS_2/NS-CNs and SnS/NS-CNs hybrid.

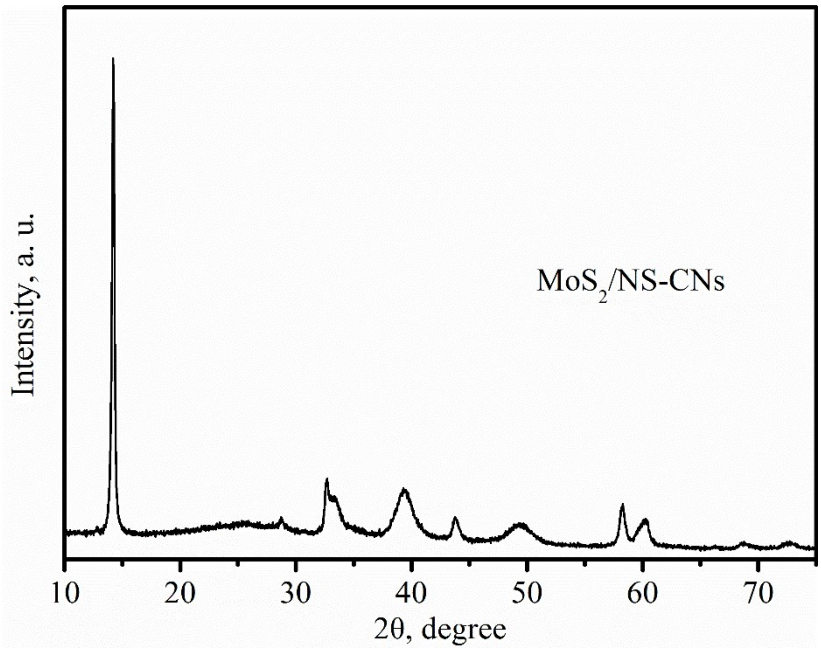

Fig. S4 XRD pattern of MoS_2/NS-CNs.

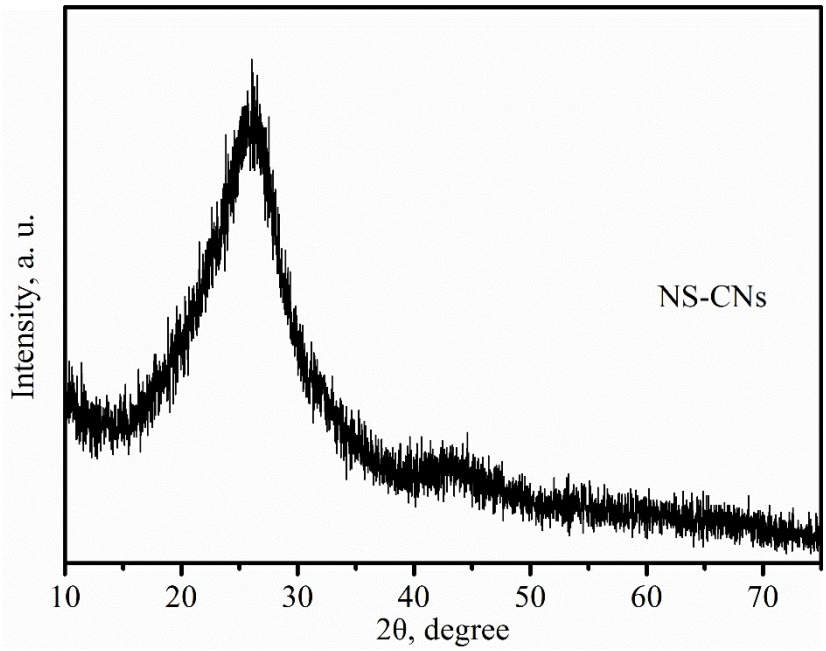

Fig. S5 XRD pattern of NS-CNs.

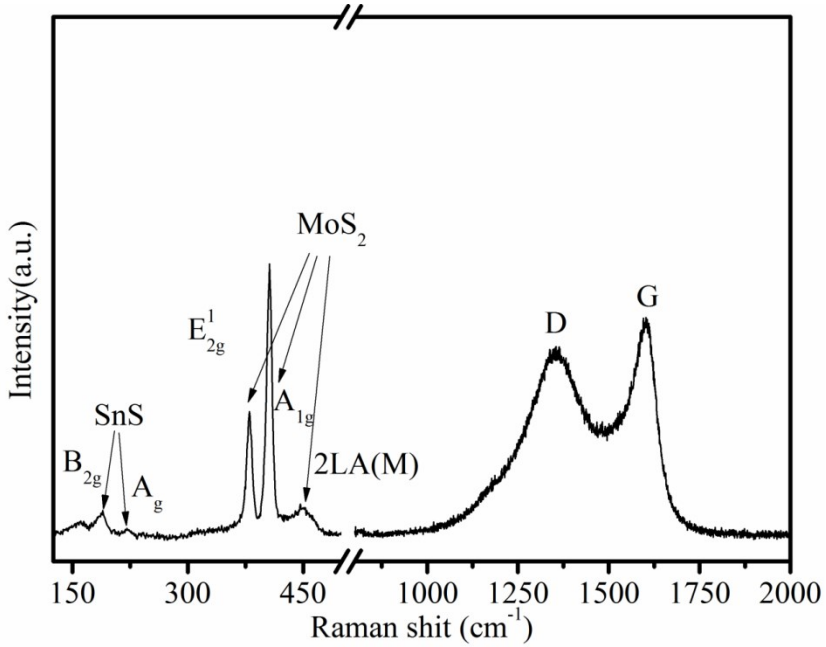

Fig. S6 Raman pattern of SnS/MoS_2/NS-CNs hybrid.

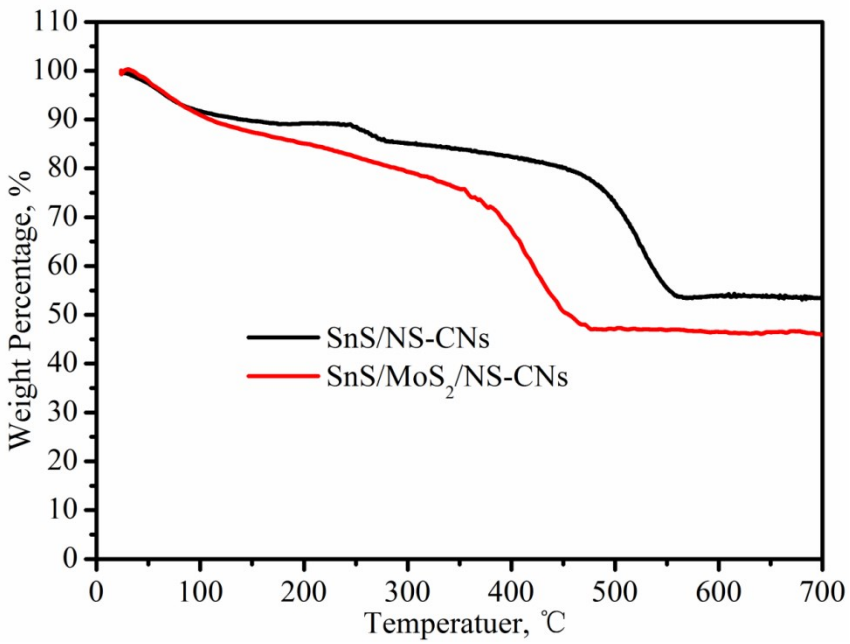

Fig. S7 TG patterns of SnS/MoS_2/NS-CNs and SnS/NS-CNs hybrid.

Table S1 ICP result of the SnS/MoS_2/NS-CNs hybrid.

Analyte	Conc.Units
Sn	42.212 mg/L
Mo	16.307 mg/L

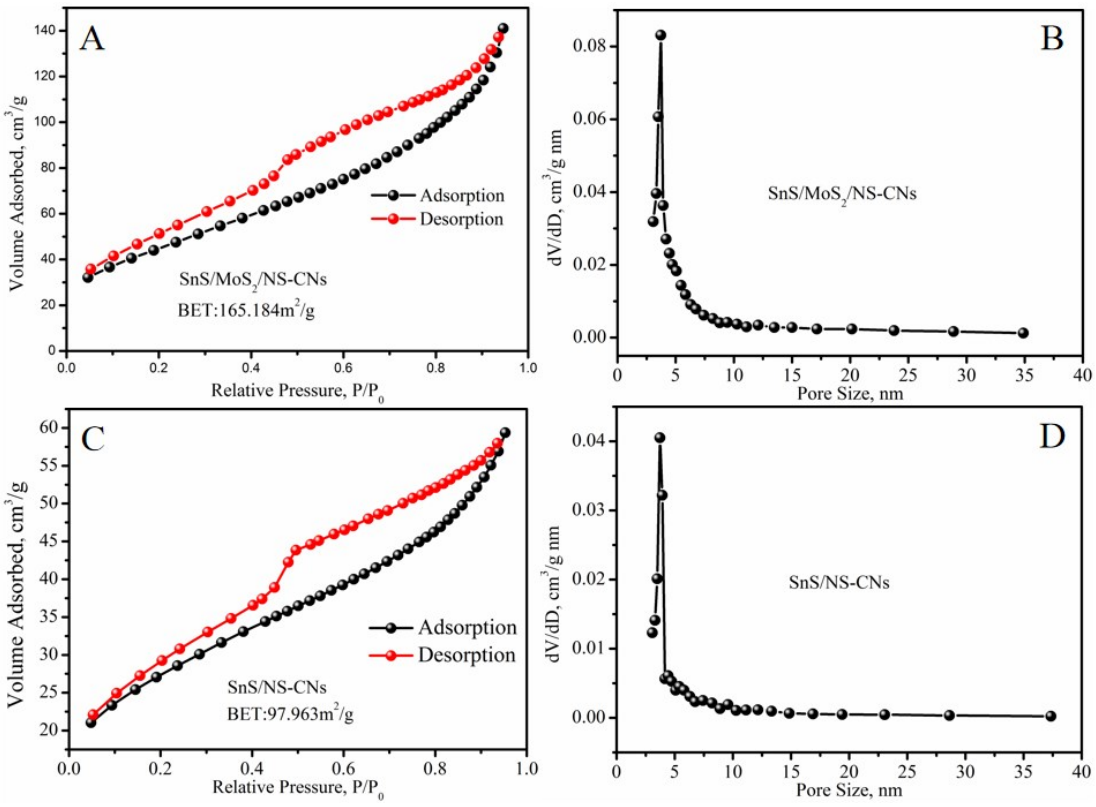

Fig. S8 N_2 adsorption-desorption iso-thermal profile and pore size distribution of SnS/MoS_2/NS-CNs (A、B) and SnS/NS-CNs (C、D) hybrid.

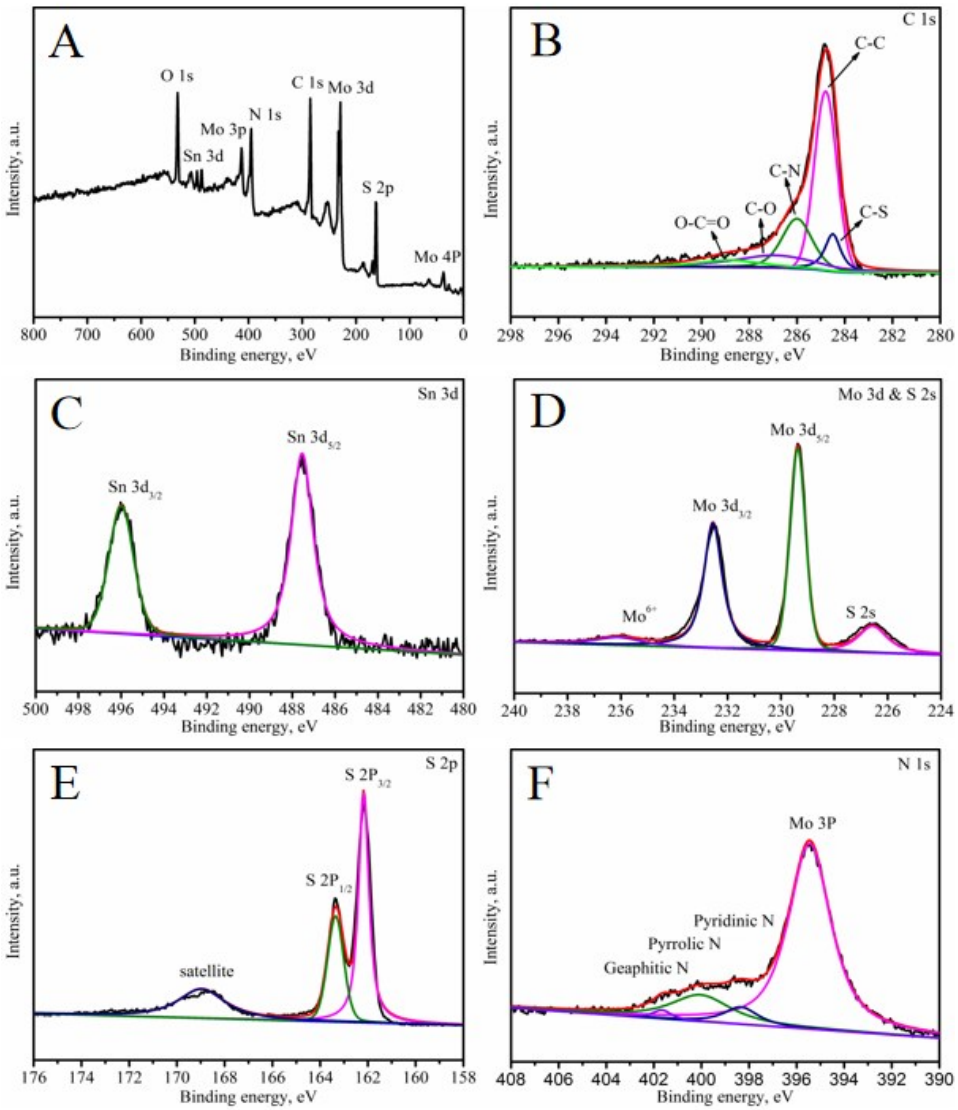

Fig. S9 XPS survey spectras of SnS/MoS_2/NS-CNs composite (A). High-resolution XPS spectra of C 1s (B), Sn 3d (C), Mo 3d &S 2s (D), S 2p (E), N 1s (F).

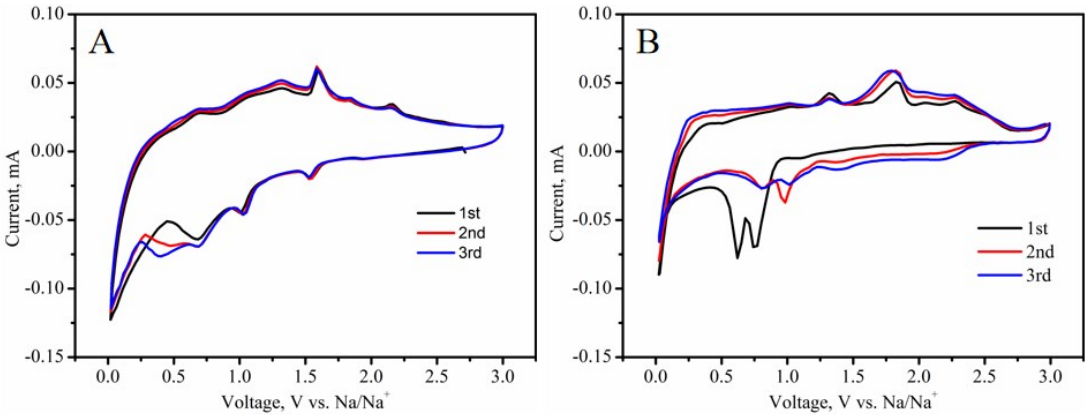

Fig. S10 CV curves of SnS/NS-CNs(A) and MoS_2/NS-CNs(B) at a scanning rate of 0.1 mV/s.

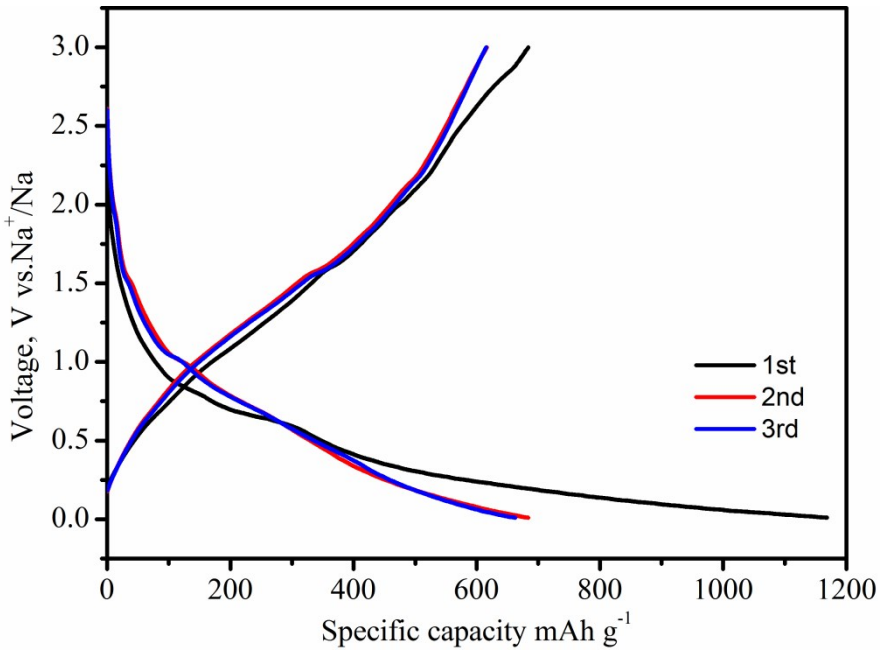

Fig. S11 typical discharge-charge profiles at 0.2 A g^{-1} of SnS/NS-CNs.

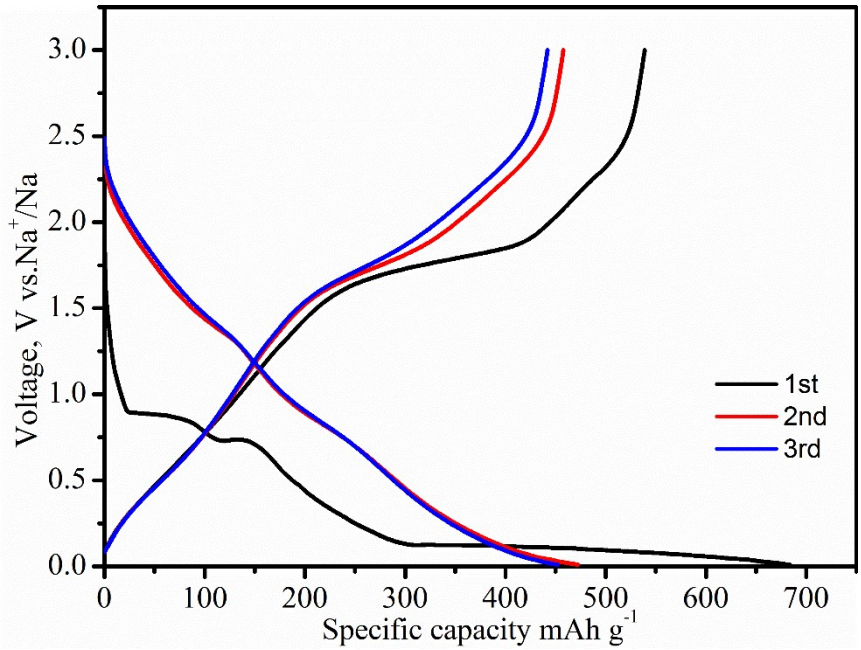

Fig. S12 typical discharge-charge profiles at 0.2 A g^{-1} of MoS_2/NS-CNs.

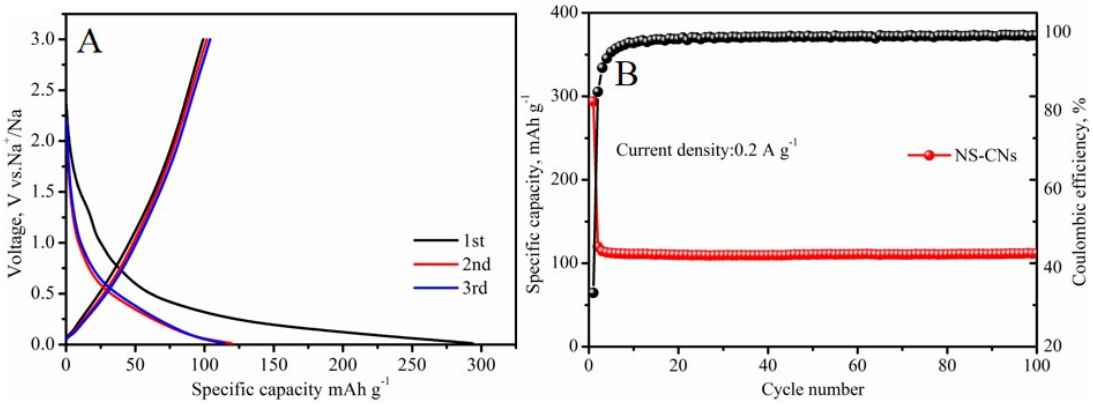

Fig. S13 Typical discharge-charge profiles (A) and cycling performance (B) at 0.2 A g^{-1} of NS-CNs.

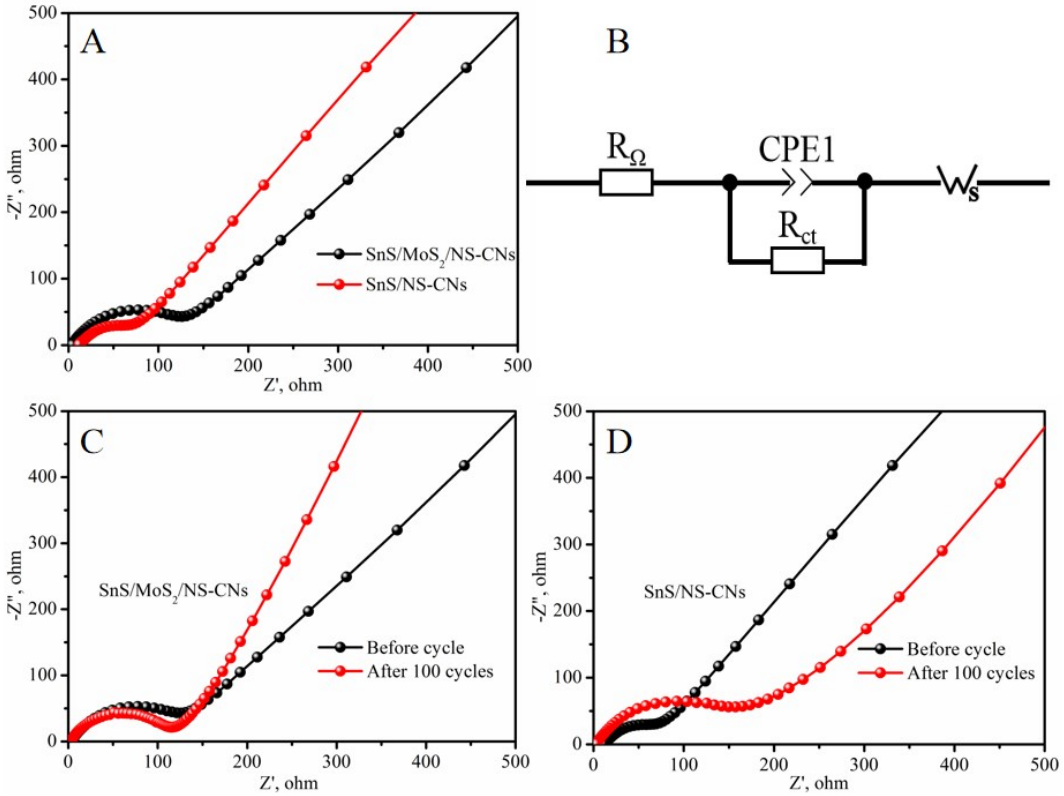

Fig. S14 Nyquist plots of the SnS/MoS_2/NS-CNs and SnS/NS-CNs (A). the equivalent circuit (B) SnS/MoS_2/NS-CNs composite after 100 cycles (C). and SnS/NS-CNs composite after 100 cycles (D)

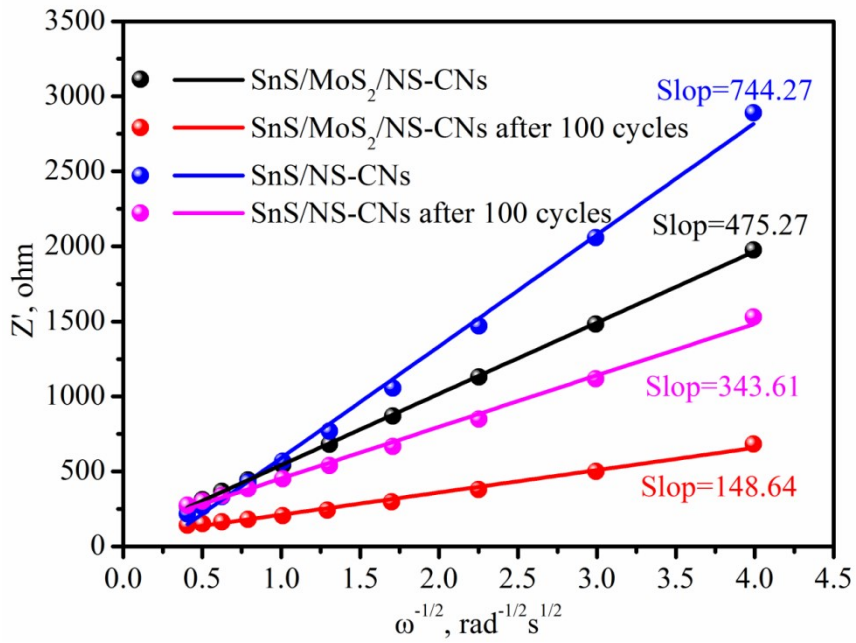

Fig. S15 The Warburg impedance coefficients (σ_w) of SnS/MoS_2/NS-CNs, SnS/MoS_2/NS-CNs after 100 cycles, SnS/NS-CNs and SnS/NS-CNs after 100 cycles.

Table S2. The ohm resistance (R_Ω) and the charge transfer resistance (R_{ct}), the diffusion coefficient of Na^+ (D_{Na}) of the SnS/MoS_2/NS-CNs, SnS/NS-CNs electrodes before and after 100 cycles.

Sample	$R_\Omega(\Omega)$	R_{ct} (Ω)	D_{Na} ($cm^2\ s^{-1}$)
SnS/MoS_2/NS-CNs	4.1	118.7	6.33×10^{-15}
SnS/MoS_2/NS-CNs after 100 cycles	3.3	115.9	1.47×10^{-13}
SnS/NS-CNs	11.4	57.3	1.99×10^{-15}
SnS/NS-CNs after 100 cycles	2.9	172.4	3.24×10^{-14}

Table S3. Comparison of the electrochemical performance of SnS/MoS_2/NS-CNs with previously reported SnS-based anode for SIBs.

Materials	Cycling performance			Ref.
	Capacity, mA h g^{-1}	Rate, mA g^{-1}	Cycles, n	
Yolk-shell SnS-MoS_2 composite	396	500	100	41
SnS nanoparticles	441.8	200	100	34
SnS QDs@NC composite	172	1000	500	29
SnS@NC composite	443	500	100	38
Yolk-shell SnS@SPC nanospheres	400	100	100	40
SnS/C nanofibers	349	200	500	42
3D SnS/C composite	400	100	100	39
SnS@C nanotubes	440.3	200	100	37
SnS microspheres[1]	364	500	50	S1
SnS/rGO composites[2]	559	200	70	S2
SnS/CNS[3]	474	1000	100	S3
SnS@C-rGO nanocomposite[4]	1027	200	100	S4
SnS/CNTs@S-CNFs composite[5]	296.6	800	600	S5
SnS/MoS_2/NS-CNs composite	**570.6**	**200**	**100**	**This work**
	287.2	**1000**	**800**	

Supplementary references

1 S. H. Choi, Y. Jang, Y. J. Choi and Y. N. Ko, *Journal of Industrial and Engineering Chemistry*, 2019, **80**, 130-135.

2 J. Li, X. Zhao and Z. Zhang, *Journal of Colloid and Interface Science*, 2017, **498**, 153-160.

3 J. Sheng, L. Yang, Y.-E. Zhu, F. Li, Y. Zhang and Z. Zhou, *Journal of Materials Chemistry A*, 2017, **5**, 19745-19751.

4 S. Zhang, G. Wang, Z. Zhang, B. Wang, J. Bai and H. Wang, *Small*, 2019, **15**, 1900565.

5 S. Zhang, H. Zhao, M. Wang, Z. Li and J. Mi, *Electrochimica Acta*, 2018, **279**, 186-194.